Journal of Power Sources 196 (2011) 5364–5376

Contents lists available at ScienceDirect

Journal of Power Sources

journal homepage: www.elsevier.com/locate/jpowsour

Electromobility concept for racing cars based on lithium-ion batteries and supercapacitors

B. Frenzel, P. Kurzweil*, H. Rönnebeck

University of Applied Sciences, 92224 Amberg, Germany

ARTICLE INFO

Article history:
Received 13 June 2010
Received in revised form 19 October 2010
Accepted 20 October 2010
Available online 27 October 2010

Keywords:
Lithium-ion secondary battery
Electrochemical supercapacitor
Electric racing car
Battery-capacitor hybrid
Service life estimation

ABSTRACT

For the construction of an all-electric race car, all aspects from engineering design over cost estimation up to the road capability are illuminated. From the most promising batteries for electric vehicle propulsion, the state-of-the art and commercial availability of lithium-ion secondary batteries is critically discussed with respect to cycle-life and unfavorable charge–discharge conditions. A market-overview is given with respect to a small electric car. Different combinations of electric motors and a recuperation system have been investigated. Weight aspects of central drive systems were considered and compared with decentralized wheel-hub drives. As a result, a centralized high-speed drive train based on a permanent-magnet synchronous engine with high-energy magnets seems to be superior due to limited space for assembly.

1. Introduction

The Formula Student competition among the universities all over the world pursues the construction of a prototype racecar. A group of students at the UAS in Amberg has been handling all aspects from engineering design over cost estimation up to the road capability of an electric car. There are three major challenges.

(1) *Design and construction.* The ambitious performance specifications of the all-electric vehicle require intensive experience in building and manufacturing, as well as considering new materials and the economic aspects of the automotive industry. The racecar must provide excellent driving characteristics such as acceleration, braking and handling. And it must be produced at a minimum of cost.
(2) *Drive train.* Different combinations of electric motors (such as induction, brushed and brushless DC or reluctance machines, gears and frequency inverters) must meet the demand of high driving performance. Weight aspects and performance of central drive systems have to be compared with decentralized wheel-hub drives. Although a recuperation system could reduce electric energy consumption, the additional equipment and weight might be considered critically.
(3) *Secondary battery.* The most promising batteries for electric vehicle propulsion have to be selected. Special attention is required by the performance data and cycle-life of lithium-ion batteries under more or less uncontrolled charge–discharge conditions.

Due to limited space for assembly, as shown in Fig. 1, a high-voltage permanent-magnet synchronous machine with high-energy magnets might be advantageous. Centralized high-speed drive trains seem to be superior at high voltages and low currents.

2. Battery concept

2.1. Challenges for the battery package

The battery package must meet the demands of different driving disciplines: Whereas skid pad, acceleration, and autocross require high electric power over short distances below 1 km, the endurance test across a 22 km distance forces a high energy battery.

The typical load profile of the endurance testing cycle is shown in Fig. 2. Average speed equals about 52.4 km h^{-1} during the acceleration periods, and 44.3 km h^{-1} during the deceleration processes. Whereas top speed was at 85.5 km h^{-1}, the most frequent velocities range between 30 km h^{-1} and 60 km h^{-1}. Maximum acceleration reaches roughly 19 m s^{-2} (about 2 g). To accelerate the vehicle, instantaneous specific power, $P_s(t) = a(t) \cdot v(t)/m$, culminates at 126 W kg^{-1}, and the average specific power of 40 W kg^{-1} is required. To move a car weighing 365 kg, this corresponds to an average drive power of 14.6 kW, and an energy demand of 6 kWh for a 25 min endurance race. Air drag and rolling resistance are discussed in Section 2.3.

* Corresponding author. Tel.: +49 09621 482 154; fax: +49 09621 482 145.
E-mail address: p.kurzweil@haw-aw.de (P. Kurzweil).

0378-7753/$ – see front matter © 2010 Elsevier B.V. All rights reserved.
doi:10.1016/j.jpowsour.2010.10.057

Nomenclature

A	equivalent frontal area of the vehicle (m^2), specific electric loading ($A\,m^{-1}$)
B_δ	magnetic flux density in air gap (T)
C	capacitance (F)
c_w	aerodynamic drag coefficient (–)
DoD	depth of discharge (%)
F_L	Lorentz force (N)
g	gravitational acceleration: 9.81 $m\,s^{-2}$
I	electric current, winding current (A)
l	magnetically active machine length (m)
m	mass of the vehicle (kg)
n_N	nominal speed, number of revolutions per minute (min^{-1})
P	electric power (W)
P_N	nominal power (W)
p	number of machine poles (–)
R	resistance (Ω)
r	bore radius (m)
T_N	nominal torque (Nm)
T_E	electromechanical torque (Nm)
U	electric voltage (V)
v	vehicle velocity ($m\,s^{-1}$)
x	flat projection: $x = r\,\theta$ (m)
W	energy (J)
z	total number of conductors (–)
α	gradient angle of the road (deg)
θ	angle (rad)
μ	rolling resistance coefficient (–)
ψ	flux linkage (V s)
ρ	air density ($g\,m^{-3}$)
τ_p	pole pitch (m)
ω	angular frequency ($rad\,s^{-1}$)

Motorcars consume 3–4 l gasoline for this performance, as we know from our earlier racing experience. With the heating value of fuel, and an overall efficiency of the internal combustion engine of roughly 30%, the fuel consumption corresponds to an energy demand for the race of about

$42{,}500\,J\,g^{-1} \cdot 0.74\,g\,cm^{-3} \cdot 3500\,cm^3 \cdot 30\% \approx 9.2\,kWh.$

Supposing an electrical efficiency of the traction system of close to 90%, and a realistic voltage drop of battery voltage of 20% during discharge, the battery requires a stored energy of about 12 kWh, corresponding to, e.g., 600 V and not more than 20 Ah.

The battery package, according to Fig. 3, consists of a series combination of several battery modules, in which a number of single batteries is connected in parallel. The series combination supplies the required voltage for the electric engine. The parallel combination improves battery capacity to meet the requirements of the endurance race. A constant peak performance of 580 V, and 100 A for a duration of 25 min, requires an unrealistically big battery (24.2 Wh, 41.7 Ah). Based on 260 commercial 22.2 V/4 Ah lithium-ion modules ($n = 26$ in series, $z = 10$ in parallel), this 40 Ah battery pack would weigh 172 kg at a volume of 89 l, except connections and cables.

2.2. Cell chemistry

The secondary battery must meet the following requirements:

- General safety during operation and handling
- High specific energy and efficiency
- Maximum discharge current of 100 A, and high current density for recuperation
- Small voltage drop under current load
- Low cost

The regulations recommend that each accumulator is monitored by a battery management system during charge and discharge, which monitors the cell voltage of every cell to keep the cells inside at the allowed minimum or maximum cell voltage. Continuous temperature measurement shall prevent the accumulator from thermal runaway.

2.2.1. Battery type

Table 1 compiles the specific characteristics of current battery systems for an application in a small electric car. With respect to specific energy and power, current battery technology recommends lithium-ion batteries (about 100 Wh kg^{-1} at 500 W kg^{-1} for 1000 s), followed by nickel–metal hydride. Nickel–cadmium technology involves environmental concerns, lead-acid batteries are far too heavy (about 10 Wh kg^{-1} at 500 W kg^{-1} for 100 s). Volume and weight play the most important role for the electric racing car, whereas cycle life and shelf life are less important.

2.2.2. Lithium-ion technology

Unfortunately, appropriate low-cost lithium-ion batteries for electrotraction are hardly available on the market. In Table 2, a market overview of current secondary batteries of various manufacturers is given with respect to suitability for the E-car project. Cylindrical cells are good at maintaining a high mechanical pressure and stability. Prismatic housings allow large formats cells and high surface area, especially pouch-type cells (coffee-bag design). Market prices per single lithium-ion cell range between about 1.30 EUR Ah^{-1} and 11 EUR Ah^{-1}.

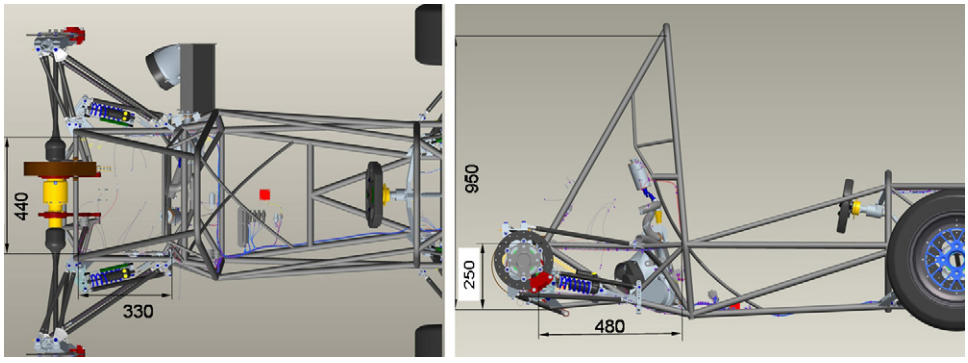

Fig. 1. Limited space for the electric propulsion system.

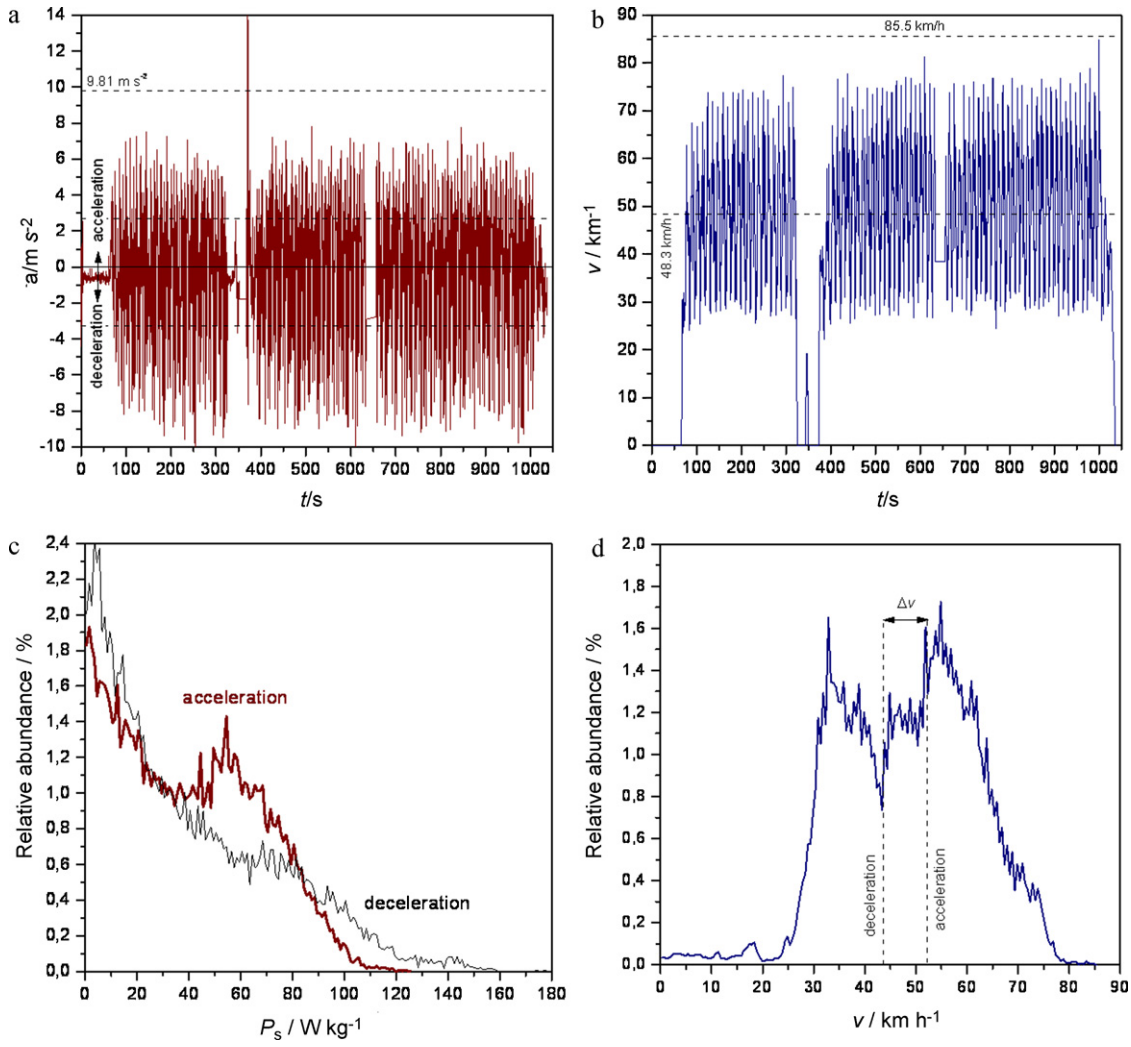

Fig. 2. Load demand of the electric traction system based on measured motorcar racing data. (a) Longitudinal acceleration versus time, (b) velocity over time, (c) distribution of specific power in time, (d) distribution of speed in time.

With respect to specific energy, the racing team decided in favor of a series combination of commercially available KOKAM batteries. The 11 Ah cell is offered at a price of about 43 EUR. Repeated charging at high pulse currents is limited by the cell chemistry based on lithium nickel manganese cobalt oxide (NMC cathode) and a graphite anode, so that additional supercapacitors have to be considered for the regenerative braking concept.

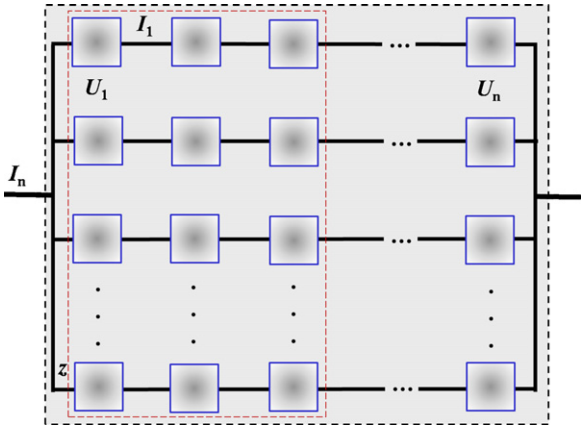

Fig. 3. Battery block comprising several 120 V modules (dashed). In total, $n = U/U_1$ single batteries are connected in series, and $z = Q/Q_1$ in parallel, according to the desired electric voltage U and capacity Q.

With respect to the power demand of the vehicle, lithium iron phosphate appears to be the best choice, providing very high rate, fast charge, and long cycling [1]. At wholesale, the number of 188 LiNANO 3.2 V batteries required for the 600 V engine is offered at the remarkable amount of money of 4100 EUR (12 Ah) or 5600 EUR (16 Ah), respectively. These cells can be continuously discharged at 5 C, i.e. at 60 A and 80 A, respectively, until the cutoff voltage of 2.1 V is reached. Depending on the internal resistance of $R = 0.011\ \Omega$ ($0.005\ \Omega$), $I^2R \approx 40$ W (32 W) of Joule's heat must be removed by air cooling during the race. For peak power requirements, 10 C = 120 A (160 A) are delivered instantaneously. The 600 V battery pack requires a mass of at least 74 kg (94 kg) and a volume of 52 l (68 ℓ) including mounting. The charging current is limited to 3 C (36 A) and 5 C (80 A), which does not allow the recovery of momentary braking power in every driving situation. See discussion below.

The lithium-ion cells of SAFT (3.6 V, 7 Ah) make up a powerful alternative to overseas manufacturers. Graphite-based anodes and nickel oxide-based cathodes in an electrolyte of $LiPF_6$ in organic carbonates deliver continuous currents of 100 A, and current peaks of 250 A for a period of 10 s. The battery price for individual electric cars, including thermal and safety management, is currently fired by the medium-term demand in automotive industry.

Table 1
General overview of battery technologies with respect to the application in a small electric racing car (compiled from different sources) [1].

	Li-ion: cathode materials (+)						Ni–MH	Ni–Cd	Lead-acid
	$LiCoO_2$	NCA	NMC	$LiMn_2O_4$ spinel	$LiFePO_4$ olivine	Polymer			
Nominal voltage (V)	3.7	3.5	3.7	~3.75	~3.25	3.7	1.2	1.2	2.0
Voltage limit on charge (V)	4.2	4.2	4.4	4.2	3.6	–	1.3	–	2.0
Theoretical specific capacity (Ah kg^{-1})	137	–	~250	148	165	–	209	180	83.5
Specific energy (Wh kg^{-1})	~165	~230	~140	~115	~115	~165	~60	50	35
Specific power (W kg^{-1})	350. . .2200					3000	250–1000	150	180
Charge/discharge rates									
a) continuous	≤1 C	≤ 1C	(a) ~5 C	(a) 10 C	(a) 30 C	(a) 0.5 C	–	–	–
b) pulse			(b) 30 C	(b) 40 C	(b) 80 C	(b) <30 C			
Temperature range (°C)	–20. . .60						–10. . .50	–40. . .50	–25. . .60
Memory effect	No						Yes	Yes	No
Charge characteristics	Constant current, voltage limited (>1.6 V)						Constant current		
Overcharge	Damages cathode, thermal runaway						Tolerant		
Discharge characteristics	Sloping: voltage drops in cold, at high discharge current, and low state of charge. Enables deep cycling (>80% DoD). Tolerates microcycles						Flat		
Overdischarge	Plates lithium metal. Low-voltage threshold						Tolerant		
Cycle life	800. . .2500. Capacity loss during cycling						<2500	1000	100. . .1000
Self-discharge (% $month^{-1}$)	< 3. . .10						<1. . .15	10. . .20	2. . .5
Battery price	High						Medium	Medium	Low
Safety risk	Electrolyte fire, thermal runaway, low recharging safety						Fire, thermal runaway	Toxic metal	Hydrogen generation
Precautions	Burst disc, fire wall, single-cell monitoring, protective circuitry						Burst disc, ventilation	–	vent, ventilation
Lifetime (years)	4.5. . .9						2. . .4	–	1.5. . . 3

NCA = lithium nickel cobalt aluminum, $LiCo_xNi_yAl_zO_2$.NMC = lithium nickel manganese cobalt; NCM = lithium nickel cobalt manganese, $LiCo_xNi_yMn_zO_2$; Ni–MH = nickel/metal hydride C-rate = discharge time × capacity.

Table 2
Incomplete market overview of secondary batteries, compiled from data available by manufacturers.

Manufacturer Battery and Technology	Specific energy (Wh kg^{-1})	Rated voltage (V)	Rated capacity (Ah)	Current at discharge/charge (A)	Mass (kg)	Volume (mm^3)
Lithium-ion secondary batteries						
A123: 26650 ($LiFePO_4$)	108	3.3	2.3	70/10 (>1.6 V)	0.070	Ø 25 × 65
Enax (LíMnO)	138	3.8	20	100/40	0.55	325 × 129 × 8
Kokam SLPB 11543140H5 (NCM)	144	3.7	5	150/10 (>2.7 V)	0.128	142 × 43 × 12
Kokam SLPB 55205130H	139	3.7	11	55; 110 peak/22 (>2.7 V)	0.292	130 × 206 × 6
Lipopower LiNANO SL-FHW 38140SE ($LiFePO_4$)	97	3.2	12	60; 120 peak/36 (>2.1 V)	0.395	Ø 38 × 154
Lipopower LiNANO SL-FHW-40160SE ($LiFePO_4$)	102	3.2	16	80; 160 peak/80 (>2.1 V)	0.50	Ø 40 × 172
Panasonic NCR18650	220	3.6	2.9	9/–	0.046	Ø 19 × 65
Saft VL7P	67	3.6	7	100/– (>2.0 V)	0.37	Ø 41 × 145
Saft VL20P	89	3.6	20	250/– (>2.0 V)	0.80	Ø 54 × 163
Samsung 18650	190	3.7	2.6	5/2.6	0.05	Ø 18 × 65
Sanyo 18650	191	3.7	2.5	–/1.7	0.047	Ø 18 × 65
Sony 26650VT	100	3.6	2.5	30/–	0.090	Ø 25 × 65
Nickel–metal hydride						
BatteryCombo NiMh	68	12	20	50/–	3.2	337 × 68 × 61
Colorado NiMh	52	48	20	50/–	18.1	132 × 132 × 279
Lead–acid						
Powersonic AGM	34	12	7	–	2.5	151 × 94 × 65
EnerSys CYCLON 0820-0020	29	12	25	–	10.4	205 × 138 × 184

2.3. Lithium batteries in pulse power operation

Electrotraction and regenerative braking face the specific safety risks and cycle life problems of lithium-ion batteries, which do not tolerate both trickle charge and float charging, i.e. continuous, long-term charge to maintain the fully charged state. If charge rates are too high, lithium metal can be plated at the negative electrode, which leads to rapid cell capacity fade. Active equalization circuitry is needed to keep all the cells within a lithium-ion pack in a similar state-of-charge.

During regenerative braking, a high current density is fed to the battery in pulses. The question is, whether the short rest periods between charging and discharging pulses allow the chemical reaction in the lithium-ion battery to stabilize and equalize throughout the electrode bulk. Currently, manufacturers define a CC–CV charging procedure, i.e. constant-current charging, followed by a constant-voltage charging to avoid overcharge. It is known that 'burp charging' using intermittent discharge pulses avoids the growth of dendrites and may improve the release of gas bubbles in batteries. As well, intermittent 'on–off' charging seems rather to prevent overcharging than to be harmful to the battery.

However, the charge rate is limited by solid-state diffusion of lithium ions into the bulk of the active mass particles. High surface-to-volume ratio materials favor high-rate capability, but, on the contrary, the tortuosity of mass transport is increased. Mechanical stress during cyclic insertion and extraction of lithium ions promotes pulverization and leads to a loss of electronic conductivity between the particles. Li^+ concentration gradients, during high charge or discharge rate, cause undesired overpotentials determined by mass transport. Nevertheless, pulse charging was reported to be helpful in eliminating concentration polarization and increasing the power transfer rate and active material utilization and reversibility [2].

With respect to safety issues including overcharge and overdischarge of individual cells, fire and explosion, we consider the pulsed operation of lithium-ion batteries to be insufficient for our electric race car. We determined to employ a supercapacitor for load-leveling and regenerative braking.

2.4. Regenerative braking and load leveling

With respect to an effective propulsion system of low weight, the regeneration of braking energy appears to be favorable. The power demand of the vehicle is theoretically given by the road–load Eq. (1).

$$P = \underbrace{\frac{1}{2}\rho c_w A v^3}_{\text{arodynamicd drag}} + \underbrace{\mu m g v}_{\text{rolling resistance}} + \underbrace{m v \frac{dv}{dt}}_{\text{accerlation and deceleration}} + \underbrace{mg v \sin\alpha}_{\text{climbing or descending}} \quad (1)$$

The symbols are compiled in a separate list. On a runway of 22 km length, 9.2 kWh of mechanical energy correspond to an average driving resistance of roughly 1500 N. At a constant speed of 100 km h^{-1}, rolling friction of about $F_\mu = 0.03 \cdot 300\,\text{kg} \cdot 9.81\,\text{m s}^{-2} \approx 90\,\text{N}$, and air drag of $F_a = ½ \cdot 0.3 \cdot 1.5\,\text{m}^2 \cdot 1.3\,\text{kg m}^{-3} \cdot [(100/3.6)\,\text{m s}^{-1}]^2 \approx 226\,\text{N}$, appear to be small against the remaining 'acceleration resistance' to reach the desired speed.

About 30% of the braking load occurs at the rear drive axle, and 70% at the front axis, that could partly be recovered with an efficiency of 84% by the motor–inverter combination. Roughly estimated for a car, weighing 365 kg, regenerative braking from 100 km h^{-1} to halt at an overall efficiency of $\eta = 25\%$, supplies an energy of

$$W = \eta \cdot \frac{1}{2} m v^2 \approx 35\,\text{kJ}, \quad \text{or } 83\,\text{Wh}$$

to be stored either in a battery or a supercapacitor. As batteries critically face the problem of high charging currents (cf. Section 2.3), a series combination of supercapacitors might be sufficient to meet the high-power requirement.

In a regenerative propulsion system based on an electric motor working between 400 V and 810 V), a module of 300 commercially available 360 F supercapacitors ($C = 1.2$ F), working in the said voltage window, is able to store

$$W_1 = \frac{1}{2} C[U_0^2 - U_1^2] \approx 298\,\text{kJ}, \quad \text{or } 83\,\text{Wh}$$

of braking energy and overrun (engine braking). On discharge, the internal resistance of the capacitor bank, $R \leq 0.96\,\Omega$, and the discharge current of 100 A must be considered.

$$W_2 = \frac{1}{2} C[(U_0 - IR)^2 - U_1^2] \approx 210\,\text{kJ, or } 58\,\text{Wh}$$

Unfortunately it holds that: the higher the discharge current, the lower the withdrawable energy. The internal resistance of each single capacitor must be lower than 0.01 Ω to allow efficient regenerative braking.

The capacitor is most efficient between the rated voltage U_0 and $U_0/2$, whereby 75% of the stored energy becomes available. The discharge efficiency equals

$$\alpha = 1 - \frac{IR}{3/4 U_0} \approx 84\%,$$

which enables a peak power of

$$P = \frac{9}{16}(1-\alpha)\frac{U_0^2}{R} = \frac{3}{4} U_0 I \approx 61\,\text{kW}$$

for a period of almost 5 s.

2.4.1. Hybrid system

The supercapacitor bank allows the battery capacity to be designed smaller and at lower system cost. According to our calculations, in a hybrid system, as shown in Fig. 4, the additional mass of the capacitor module (1.2 F, 400–810 V, 20 kg, 5.4 Wh kg^{-1}) is compensated after approximately 14 recuperation events, from 80 km h^{-1} to halt at an efficiency of only 25%.

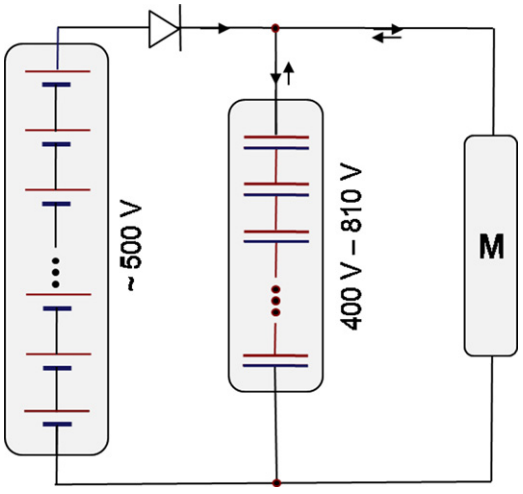

Fig. 4. Hybrid system of a lithium-ion battery (50 Wh kg^{-1}) and a bank of supercapacitors (300 pieces of 360 F, 2.7 V, 5.45 Wh kg^{-1}), connected to an electric engine (generator). Startup circuit neglected.

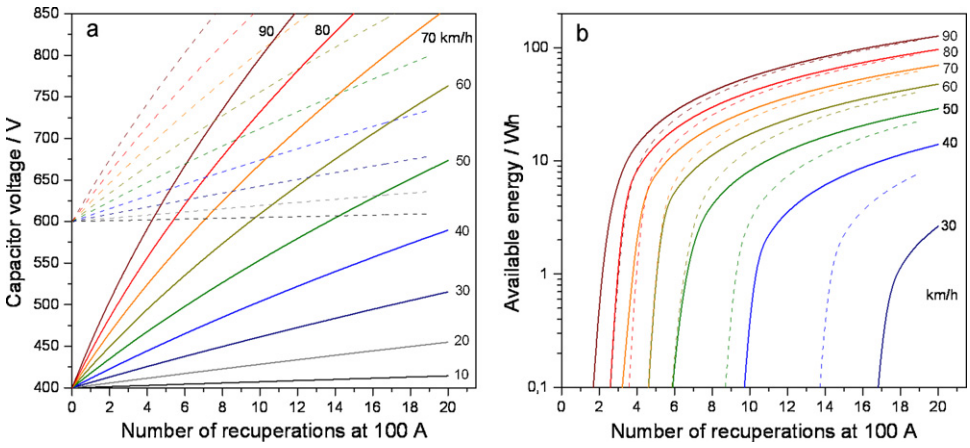

Fig. 5. Repeated regenerative braking of an electric car (mass 365 kg) from different velocities to halt, at a system efficiency of 25%. (a) Increase of voltage at a module of 300 individual supercapacitor cells (100 F, 2.7 V), initially charged to 50% of the rated voltage (solid lines), and charged at 75% (dashed). (b) Withdrawable energy at constant current discharge of the supercapacitor module (internal resistance 1 Ω).

In combination with a 600 V battery module (6.9 Ah, 39 kg, 18 l) of 546 single cells in series and in parallel, the supercapacitor improves the specific mass of the hybrid system by about 1.1 Wh kg^{-1} with every full charge by 14 recuperation events. The fully charged capacitor bank is able to deliver a peak power of 60 kW for about 5 s.

Fig. 5 gives an overview of the withdrawable energy which is delivered by the supercapacitor bank under different deceleration conditions. In this worst-case scenario, at 25% efficiency of the recuperation system and a constant current power demand of 100 A, the specific power of the battery–supercapacitor hybrid system is doubled after about 500 recuperation events from 90 km h^{-1} to halt.

We conclude that the supercapacitor appears to be most useful for a large number of short braking events and deceleration periods at high currents, i.e. under conditions that cause serious problems with lithium-ion batteries.

2.5. Selection of supercapacitors

So-called double-layer capacitors [3] allow fast charging and discharging at high currents of several hundred Amperes over almost one million of cycles. A pulse power capability in the range of 5 kW kg^{-1} predestines activated carbon powder electrodes in highly conductive organic electrolytes for regenerative braking as long as high-current compliant lithium batteries are not commercially available.

2.5.1. Rating

Preferred supercapacitors for the electric car from different manufacturers are compiled in Table 3. NESSCAP 360 F/2.7 V supplies a maximum current of 226 A at a stored energy of 0.365 Wh, and a leakage resistance of 3600 Ω.

We assume a relationship between low selfdischarge and good aging stability. For example, the WIMA capacitor exhibits a voltage drop of less than 0.1% per day after full charge, and shows a superior stability of capacitance even at 65 °C, namely ≤−0.0015% per hour at 2.5 V.

2.5.2. Life and stability

Under the conditions of regenerative braking, supercapacitors age by gradual increase of resistance and loss of capacitance [4]. Interruptions bring about a temporary recovery of storage capability, but do not basically alter the long-term trend of pulse power operation; cf. Fig. 6(a).

In the aged supercapacitor, parasitic currents arise without capacitive use for energy storage. Fig. 6(b) demonstrates that the undesired residual charge at the end of the discharge ramp at a cell voltage of 0 V must be neutralized by the subsequent charging ramp. The stored charge at 2.7 V cannot immediately be withdrawn by the discharge current. During continuous cycling, a gradual potential shift occurs at the electrodes, until the positive electrode utilizes almost the entire voltage window, and the potential changes at the negative electrode get smaller and smaller [5].

The deterioration of capacitance does not allow any reliable estimation of service life until an appropriate fit function is defined after several years of testing. Therefore, we observe the gradual growth of the relative time constant function over time t as an early indicator of failure [6].

$$\frac{\tau(t)}{\tau_0(t)} = \frac{R(t)\cdot C(t)}{R_0(t)\cdot C_0(t)}$$

R_0 and C_0 denote resistance and capacitance of the virgin capacitor. The product of relative capacitance loss C/C_0 and resistance increase R/R_0 over time is easily available from discharge characteristics or impedance spectra. The peak F in Fig. 6(e) marks the predicted life-time after the shortest possible time of testing.

With this, we selected the capacitors' sizes and brands under the specific testing procedures and life-time projections of the electric car.

Table 3
Rated data of commercial supercapacitors and modules.

Manufacturer	Rated capacitance (F)	Rated voltage (V)	Specific energy (Wh kg^{-1})	Volume (L)	Mass (kg)	Series resistance (Ω)
Nesscap ESHSR	360	2.7	5.57	0.068	~0.066	<0.0032
Nesscap EMHSR	62	125	2.36	~75	57	<0.015
Maxwell BCAP	350	2.7	5.62	0.053	0.063	0.0032
Maxwell MBOD	63	125	2.53	~86	59.5	0.018
Wima	300	2.5	3.0	0.075	0.090	0.006

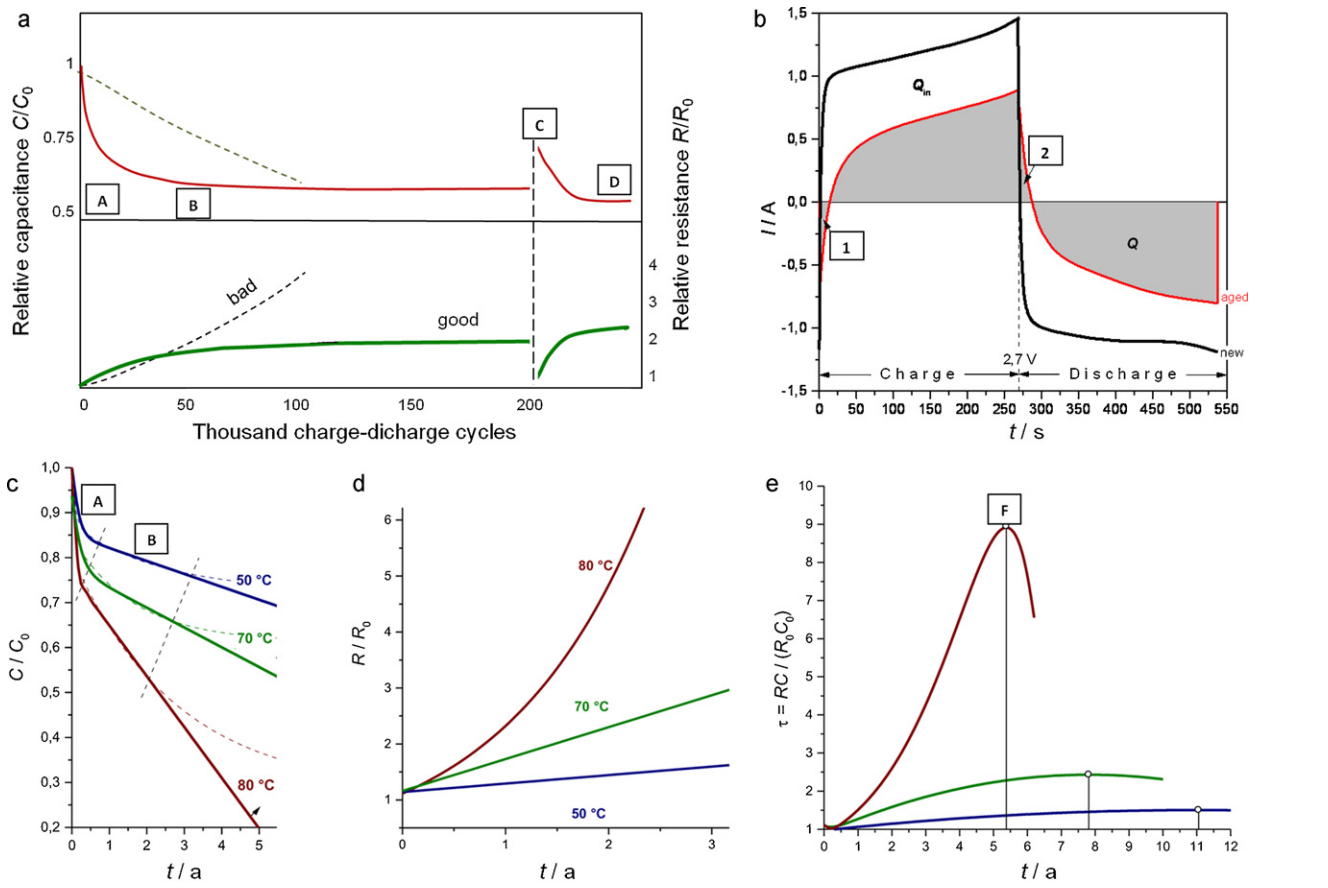

Fig. 6. (a) Pulse-power characteristics of activated carbon supercapacitors and series combinations thereof: A, run-in period; B, aging; C, interruption; D, after recovery. (b) Loss of storage capacity and parasitic residual charges (1, 2) in the cyclic voltammogram of a 100 F/2.7 V supercapacitor after long-term testing at 2.1 V and 80 °C; $Q = -151$ As; $Q_{in} = 160$ As. Scan rate 10 mV s^{-1}. (c)–(e) Service life estimation by means of the maximum (F) of relative time constant, i.e. the product of capacitance loss and resistance increase during long-term testing at different temperatures.

3. Electric drive

Two approaches were investigated to minimize the weight of the electric drive system.

(1) Water cooled high-speed motors provide low machine diameters and low weights in combination with low motor currents at a given operating point. As a consequence, low motor currents and low copper mass for wiring are necessary for high power applications. Unavoidably, high-speed systems show a considerable drive gear with high transmission ratios due to kinematic and kinetic restrictions. As long as low-voltage battery packs are used, in addition to the heavy water cooling system and electronic components such as boost converters, this will increase cost and weight.
(2) Convective or fan air-cooled systems having a reduced gear head might be an alternative solution. The absence of water and the heavy gearbox, and missing boost converters result in weight benefits for these low-voltage, high-current direct-drive systems. This is contradictory to the increase in mass, because of the increase of wiring and machine diameters.

The system overview of the realized electrical drive train for the student racing car is shown in Fig. 8(a). The motor is driven by an inverter to adjust speed or torque, and is fed by a DC link connected to the battery packs. In braking phases, the motor works as a generator, and recuperates mechanical energy back to a storage pack. Thereby, an optional chopper circuit can activate a braking resistor to limit the DC link voltage. The storage pack may consist of batteries and supercapacitors, which limit voltage peaks and absorb short time charge–discharge cycles [7]. There are two approaches for this hybridization, whereby the external parallel hybrid (EPH), as an external hardwired parallel connection of batteries, and capacitors seems to be most promising [8]. For the motor, different types can be chosen, although only a limited number may be applicable for the project.

3.1. Electric motor

For a drive train in the racing car, different combinations of electric motor, inverter and gear can be found. Traditionally, the electric motor marks the starting point in comparing different solutions. Selecting the components focuses on volume and weight of the total system. Nevertheless, different aspects, such as cost and availability, cannot be neglected, although they play a minor role in the selection process. In this paper, the number of different motors has been limited to the most common DC and AC motors practically used:

- Induction Machine or Asynchronous Machine (ASM)
- Permanent Magnet Synchronous Machine (PMSM)
- Brushless DC Machine (BLDCM)
- Brushed DC Machine (BDCM)
- Switched Reluctance Machine (SRM)

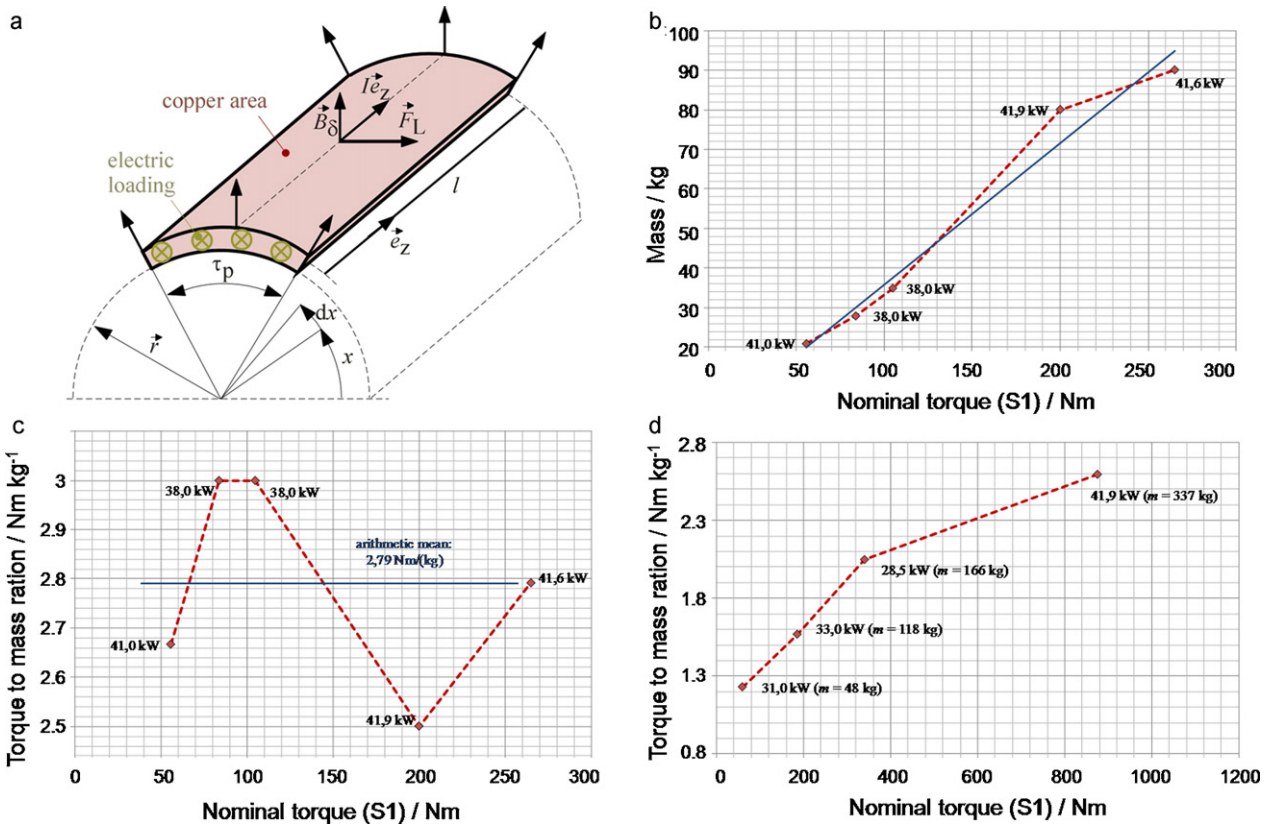

Fig. 7. Water-cooled spindle machines. (a) Torque generation in a radial flux electrical machine. (b) Mass versus nominal torque for a 40 kW synchronous machine. (c) Torque to mass ratio as function of nominal torque of a 40 kW synchronous machine. (d) Torque to mass ratio of a 30 kW asynchronous machine.

3.2. Torque to mass relation

Besides SRM, all mentioned types of motors have some fundamental principles in common with respect to volume and weight. Starting with a required mechanical nominal power P_N at the motor shaft,

$$P_N = T_N \omega_N = \frac{2\pi}{60\ \text{min}^{-1}} T_N n_N,$$

torque can be raised and speed be decreased, or vice versa. The source of the generated nominal torque T_N, the electromechanical torque T_E, is based on the Lorentz force F_L on a current-carrying conductor in an outer magnetic field:

$$d\vec{F}_L = dI(x) \cdot l\vec{e}_z \times \vec{B}_\delta(x)$$

Introducing the machine's specific electric loading $A(x)$, as shown in Fig. 7(a),

$$A(x) = \frac{dI(x)}{dx} = \frac{zI}{d\pi} = \frac{zI}{2p\tau_p} \quad \text{with} \quad d = 2r,$$

and assuming perpendicular conditions, we finally get for the total electro-mechanical torque T_E:

$$T_E = \left| \vec{r} \times \int_0^{d\pi} d\vec{F}_L \right| = \left| \vec{r} \times \int_0^{d\pi} \vec{e}_z \times \vec{B}_\delta(x) dI(x) \right|$$

$$= rl \int_0^{d\pi} A(x) B_\delta(x) dx \sim d^2 l$$

The generated torque T_E is proportional to the product $d^2 l$, and therefore to the bore hole of the used machine. Thus, for a required constant machine power, volume and weight are reduced, when torque is decreased, and speed is increased. In a first approximation, this results in a proportional relationship between nominal machine torque and machine mass.

As an example, various water-cooled synchronous machines of one model range with approximately 40 kW continuous nominal power (S1) are considered in Fig. 7(b). Such a commercially available machine [9] combines high power and low weight in a limited design space, and are generally appropriate for use as drive motors in student racing cars.

The total machine mass (sum of stator and rotor weight without cooling attachment and bearing) increases almost linearly with nominal torque, and behaves independently of nominal power. Therefore, torque to mass ratio in Fig. 7(c) remains nearly constant, and advices us to not use direct drives with a torque demand of nearly 400 Nm, but to use a combination of high-speed motor and lightweight gear.

3.3. Selection of the machine type

3.3.1. BDCM

Brushed DC Machines are used to drive electric vehicles at low acceleration demands. AC motors such as ASM, PMSM and BLDCM exhibit higher torque density, and therefore lower specific torque mass, than BDCM [10]. The brushes increase maintenance cost and reduce robustness, although special types of constructions are advantageous. For example, the so-called Lynch motor [11] is constructed as a wheel hub brushed DC motor with an inner commutator. This arrangement minimizes the circumferential speed in the commutation area and increases the rugged design for this type of motor. Nevertheless, low acceleration capabilities and less specific torque mass compared to AC machines are still a disadvantage. Therefore, BDCM are not the first choice for a small racing car,

although they are less expensive than motors equipped with high energy rare earth magnets (most types of PMSM and BLDCM).

3.3.2. ASM

The second popular type of three-phase machines, the ASM, is characterized by robustness and simple construction, rugged design, and, in the case of squirrel-cages, the absence of brushes. Nevertheless, specific mass per torque is higher than those for PMSM and BLDCM. As shown in Fig. 7(d), specific mass per torque of a commercially available water-cooled asynchronous spindle drive [12] exceeds that of a synchronous machine. For ASM, the external magnetic field is fed by current, while additional winding and cooling rise specific mass. Therefore, we consider ASM not to be the first choice for a small electric racing car.

3.3.3. SRM

The Switched Reluctance Machine is an interesting brushless candidate to drive a racing car, too. This type of motor appears to be very robust, heat resistant, simply constructed and inexpensive. Moreover, it is intensively investigated for traction drives in Hybrid Electrical Vehicles (HEV) up to a power of 50 kW [13]. The SRM is a singly excited synchronous motor with doubly-salient shapes for stator and rotor iron. It carries only copper stator windings without magnets and its operation is based on the principle of the minimum reluctance for magnetic fields. This means that, in case of a current carrying stator winding, a rotatable salient iron core will rotate to bring the stored magnetic energy to a minimum. At this position, the magnetic reluctance is also at minimum, whereas inductance seen by the exciting electrical circuit is at maximum. In this position, the next phase winding will be turned on to generate a continuous rotation.

The torque per core volume of the SRM machine is higher than that for the ASM, whereas the SRM operates at a peak air gap flux density twice as high as the peak air gap flux density of induction machines. The torque equation can be described as follows [14]:

$$T_E = \sum_{k=1}^{p} \left(\frac{\partial}{\partial \vartheta} \int_0^{I_k} \psi_k(\vartheta, \xi) \mathrm{d}\xi \right)$$

Unfavorable features are the audible noise and the torque pulsations caused by the doubly-salient mechanical structure. Reduction in torque pulsations through active phase current waveform shaping involves reduced machine efficiency. Noise introduced by radial deflection due to the high radial components of attractive forces between stator and rotor poles can be reduced with stiffer structures, but this measure increases weight. For higher power electric vehicle applications, the availability of commercial SR products appears to be rather poor and specialized, highly sophisticated, expensive inverters can be used only. This compensates the benefits compared to a PMSM and prioritizes the latter one for a racing car.

3.3.4. PMSM and BLDCM

In general, the both the PMSM and the BLDCM machine are of the synchronous type, having permanent magnets as a source for the external magnetic field. They differ in the kind of magnetization. For the PMSM, sinusoidal magnetization is applied, while for the BLDCM a radial magnetization is used. Due to higher harmonics in the latter case, the PMSM exhibits slightly better performance, although the difference is not significant. As a consequence, both the PMSM and the BLDCM show the lowest specific mass per torque of all motors, do not require brushes, and yield high acceleration values. Negative aspects are the higher price compared to BDCM, especially with rare-earth magnets, and higher temperature sensitivity compared to ASM. Nevertheless, in combination with a water-cooling system, necessary for the battery packs, we have chosen this type of machine to be the best candidate in a small racing car for the first approach.

Table 4
Inverter and motor characteristics (compiled or estimated from data sheets).

Inverter Siemens Sinamics S120 motor module	Electric motor Siemens synchronous machine 1FE1074-4WM with water cooling
Rated input current: 132 A/105 A (derating with cold plate)	Number of poles: 4
Overvoltage shutdown: 820 V (1 ± 2%)	Rated speed: 7700 rpm
DC-Link voltage range: (510...720) V	Rated power (S1): 48 kW
Undervoltage shutdown: 380 V	Rated current (S1): 97 A
Rated DC-Link voltage: 600 V	Rated torque (S1): 60 Nm
	Weight (stator & rotor): 21 kg
	Rated losses: 3.5 kW
Efficiency: 89.6%	Efficiency: 93.2%

3.3.5. Design of the drive system

Generally, reasonable design has to choose between an indirect gear drive and a direct wheel hub drive. Especially wheel hub motors formed by PMS machines, seem to be an interesting solution in applications like automotive traction systems. Their advantages are:

- rugged design,
- high torque,
- best fit in form of large diameter and short axis,
- good dynamic behavior.

Although PMS machines generate high torque, the fundamental relation between mass and weight, mentioned in Section 3.3, has to be considered. Thereby, total motor mass in the drive train is significantly increased, compared to an indirect gear drive system. For example, the PMS motor "EW20/60" [15], having a nominal torque of 85 Nm and weight of 13 kg, results in a 52 kg total motor weight for a vehicle torque of 340 Nm with four driven wheels. Although wheel hub motors are usually equipped with an external rotor to directly drive the wheels, and allow simply recuperation at motors that are installed in the front drive axis, the disadvantages have prevailed up to now: highly unsprung masses, high price and the very poor availability.

For this reason, we have not selected the wheel hub motor for the first approach. Nevertheless this type of construction will be discussed in future studies. To avoid structural alteration works, we modified an already developed racing car equipped with an internal combustion engine to be the successful basis for the electric car. The combustion engine was replaced by a central inverter/motor combination shown in Table 4. Due to the above-mentioned advantages, a commercially available PMSM spindle drive has been chosen.

3.4. Simulation of the drive train

A simplified PSpice [16] model (cf. Fig. 9) was created to simulate the behavior of the electric drive in Fig. 8(a). The load circuit is derived from the measured mechanical power required to drive an equivalent racing car powered by an internal combustion engine (cf. Section 2). Inverter and motor details were neglected, whereas we assumed constant efficiency for both parts, and ideal connections and wirings without contact and wiring resistance. To determine the required DC link voltage, the following assumptions were made:

(1) For a three-phase AC motor inverter, the rated rectified inverter DC link voltage equals usually $U_{DC} = \sqrt{2}(\sin(\pi/6))/(\pi/6)U_{12} \approx 1,35 \cdot U_{12}$.

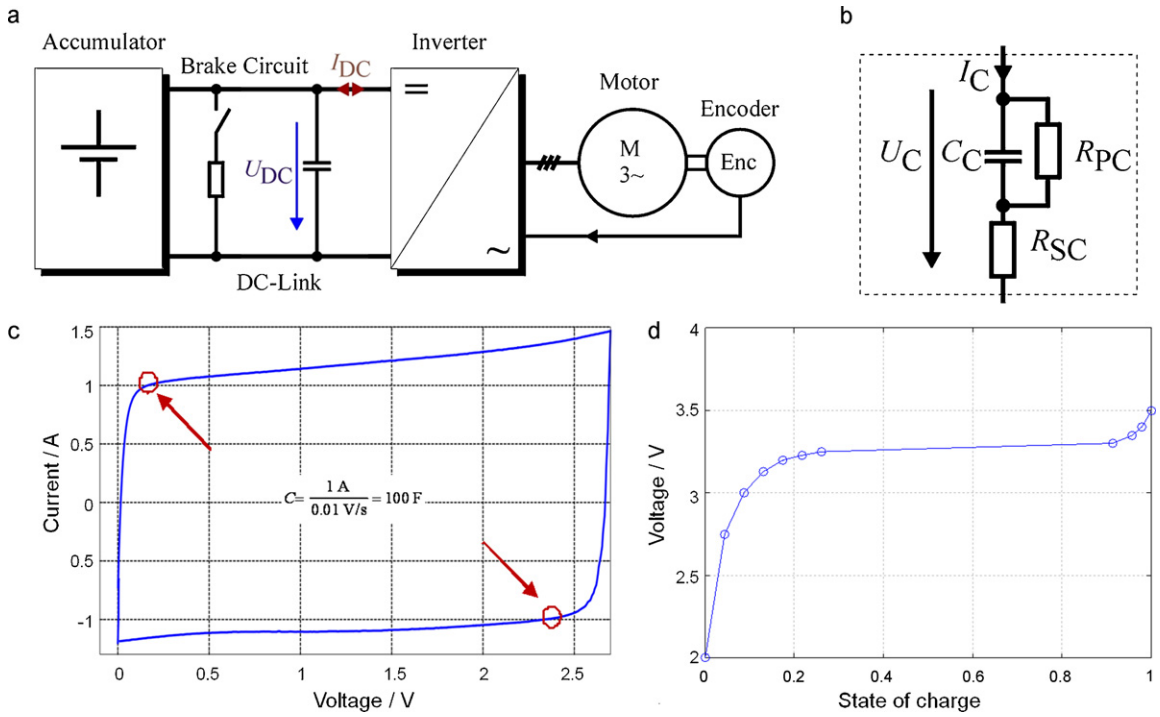

Fig. 8. (a) System overview of the electrical drive train. (b) Simplified model for supercapacitor and battery. (c) Cyclic voltammogram of a 100 F/2.7 V supercapacitor at a scan rate of 10 mV s^{-1}. (d) Nonlinear discharge characteristic of a lithium-ion battery at a discharge current of 1 A.

(2) With the European three-phase effective voltage level of U_{12} = 400 V, we get U_{DC} = 540 V for uncontrolled DC-link voltages, or even more for inverter controlled DC link voltages. Typical values range between 540 V_{DC} and 650 V_{DC}, respectively. Thus, for the simulation, we assumed a DC link voltage of 600 V_{DC}, corresponding to the rated inverter DC link voltage. This requires 6 × 30 = 180 lithium-ion battery cells (3.3 V nominal per cell) for a DC-Link voltage of about 180 × 3.3 V = 594 V in the fully charged condition, and 630 V in no-load operation (3.5 V maximum voltage per cell).

(3) The blocking diodes D1 and D4 in Fig. 9 allow the recuperation of braking energy. Advantageously, with this any sophisticated battery management system (BMS) is not required. In the recuperation mode, all energy is stored in the supercapacitor bank, which results in an increasing DC link voltage. Only in the "motor mode", when the DC link voltage U_{DC} falls below the

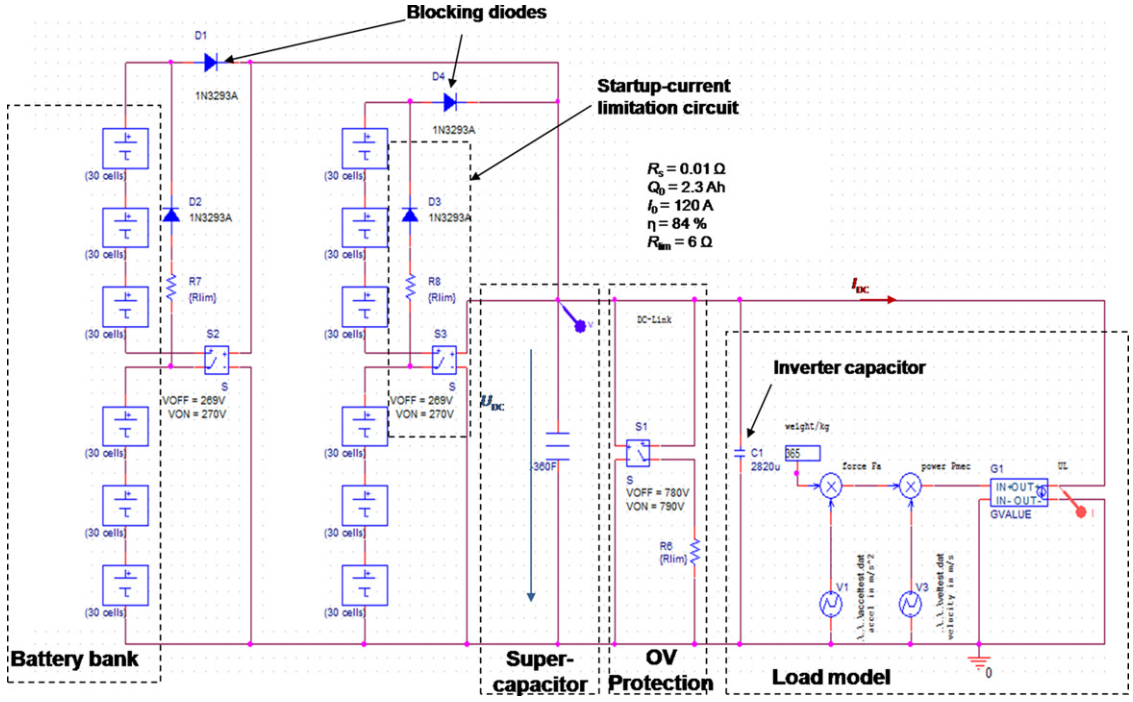

Fig. 9. Simplified simulation model for the electrical drive train.

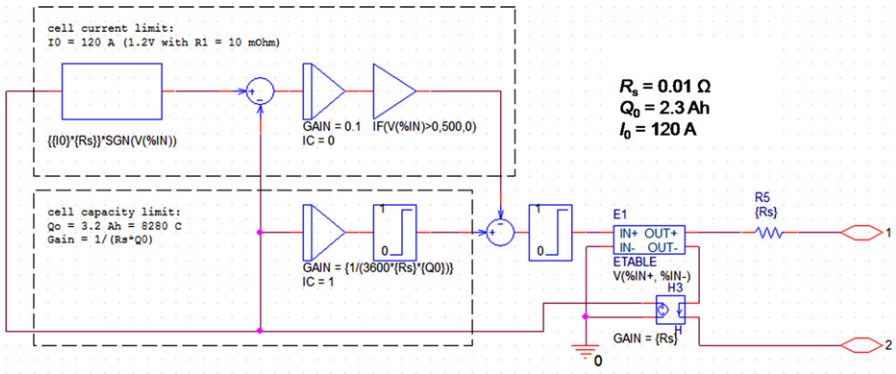

Fig. 10. PSpice model of a lithium-ion cell.

difference between the battery block voltage and the forward voltage of D1 and D2 of approximately 1.1 V, the diodes become conductive and feed both the load and the supercapacitor bank.

(4) For an overvoltage protection (OV protection), the braking circuit in Fig. 9 has been realized by the switch/resistor combination S1/R6. Switch S1 is closed even when the DC link voltage crosses 790 V. The supercapacitor bank is discharged across R6, until the DC-Link voltage will fall below 780 V.

(5) To limit startup-currents into the initially uncharged supercapacitor bank, the upper three battery banks are bypassed through the resistor/diode combinations R7/D2 and R8/D3 for a DC link voltage below $85\% \times 3 \times 30 \times 3.5\,\text{V} \approx 270\,\text{V}$. After crossing this value, the switches S2 and S3 are closed and turn on the upper three battery banks.

3.4.1. Load model

In the PSpice simulation, the electric motor and inverter combination was modeled as a variable resistance in form of a voltage-controlled current source. The motor current demand I_{DC} was deduced from the measured mechanical power profile P_{mec} (cf. Section 2), divided by the corresponding DC link voltage, with respect to a motor/inverter efficiency of $\eta \approx 84\%$:

In the motor mode ($P_{mec} > 0$): $I_{DC} = P_{mec}/(U_{DC} \cdot \eta)$

In the generator-mode ($P_{mec} < 0$): $I_{DC} = P_{mec}/U_{DC} \cdot \eta$

3.4.2. Capacitor model

The examined supercapacitor cell was modeled by a simplified first-order description, in terms of a RC connection and an additional leakage resistor in parallel to the capacitor [3], as shown in Fig. 8(b), described by the differential equation:

$$R_{SC}R_{PC}C_C\dot{I}_C(t) + (R_{SC} + R_{PC})I_C(t) = R_{PC}C_C\dot{U}_C(t) + U_C(t)$$

For the purpose of verification, cyclic voltammetry measurements were conducted at a commercial 100 F/2.7 V supercapacitor. At a voltage scan rate of $dU/dt = 10\,\text{mV s}^{-1}$, the CV in Fig. 8(c) yields a simple short time approximation for $R_P = R_S$ and $R_P C_P = t$:

$$R_{SC}C_C\dot{I}_C(t) + I_C(t) = kC_C$$

This PT_1 behavior with $(dU/dt) = C_C$ as the current excitation can be used to roughly determine the nominal capacitance of the supercapacitor, as shown in Fig. 8(c). The rated values of the preferred Nesscap capacitor are compiled in Table 3.

3.4.3. Battery model

For a commercial lithium ion cell [17], the nonlinear discharge characteristic was modeled depending on cell capacity, as shown in Fig. 8(d). The voltage drop at elevated discharge currents was realized by help of a serial DC resistance of 10 mΩ. The PSpice model is shown in Fig. 10.

The battery behavior is modeled by a voltage-controlled voltage source. By integrating the current through the battery, the normalized battery charge signal is created. Starting with a fully charged cell, the integrator's initial condition is one (IC = 1). Integrator's output is equivalent to the cell capacity that adjusts the inner cell voltage via a table-lookup. Cell current limitation was realized with a superposed delta current controller.

3.4.4. Simulation results

DC link voltage U_{DC} and load currents I_{DC} in the battery–supercapacitor hybrid system, and in the stand-alone battery system, i.e. in absence of the capacitor bank and the blocking diodes D1/D4, are compared in Fig. 11 for the typical driving cycle derived in Section 2, and in Table 5.

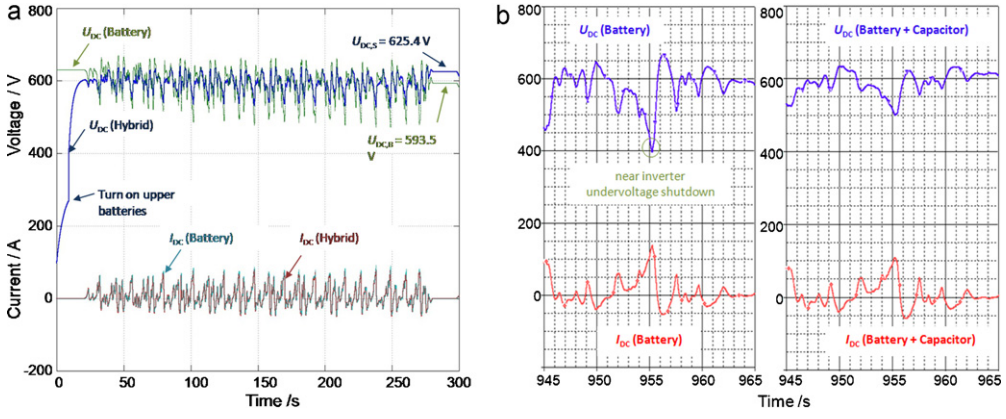

Fig. 11. Simulated driving cycle of a battery–supercapacitor hybrid system based on measured velocity data: (a) DC link voltages and load currents in presence and absence of the supercapacitor bank and blocking diodes. (b) Smoothing effect of the supercapacitor in the hybrid system on DC link voltage.

Table 5
Load currents from the battery bank at constant load profile.

Hybrid system of battery and supercapacitor	Stand-alone battery system (no D1, D4)
Mean current $\bar{I}_{DC}$: 6.09 A	Mean current $\bar{I}_{DC,1}$: 6.86 A
RMS current $I_{DC,RMS}$: 25.4 A	RMS current $I_{DC,RMS,1}$: 26.5 A
Peak current $\hat{I}_{DC}$: 81.5 A	Peak current $\hat{I}_{DC,1}$: 92.5 A

Although the equivalent series resistance of the two battery banks in parallel of $R_{iB} = 180 \times 10\,m\Omega/2 = 0.9\,\Omega$ is smaller than the equivalent series resistance of the supercapacitor bank, $R_{iC} = 300 \times 3.2\,m\Omega = 0.96\,\Omega$, the electrical energy consumption is expected to be higher for direct recuperation into the battery bank, in contrast to the supercapacitor bank. This holds because the load current $I_{DC} = P_{mec}/U_{DC}$ drops in case of constant power demand P_{mec} and increasing DC link voltage U_{DC}.

The simulated rms and mean values of the load current I_{DC} appear significantly lower in the hybrid system with the supercapacitor bank switched on. This can be understood, because the DC link voltages are higher with the capacitor bank active, due to the blocking diodes D1 and D4. Fig. 11(a) gives an example: $U_{DC,S} = 625.4\,V$ in the hybrid battery system, and $U_{DC,B} = 593.5\,V$ without supercapacitor.

Another advantage of the supercapacitor bank is its smoothing effect on the DC link voltage. The capacitor bank functions as a first-order low-pass filter with a time constant of about 1.1 s corresponding to a cut-off frequency of 0.15 Hz. This reduces the peak currents, in our example by about 12%, and extends the service life of the electronic inverter components. Without this smoothing effect, the DC link voltage may drop below 395 V and reach the critical shutdown area of the inverter, as shown in Fig. 11(b).

4. Design and manufacture

The Formula Student competition, which was founded by the Society of Automotive Engineers in 1981, pursues the concept of a fictional manufacturing company that has contracted a design team to develop a small Formula-style race car for the target group of weekend autocross racers. A team of students designs, builds, and tests a competitive prototype race car based on a series of rules, whose purpose is both to ensure onsite event operations and promote clever problem solving. In addition, costs have to be calculated with respect to a production item. Originally, the Formula Student competition addressed cars propelled by internal combustion engines. In recent years, alternative driving concepts like electric cars have been focused additionally.

4.1.1. Mechanical requirements and design history

During the events held on different locations all over the world, the teams must pass two major examinations: the first part is called "static events" including the design event, the cost event, the business case and the presentations event. Before entering the second part called "dynamic events", the ready-to-race car has to pass a deep inspection insuring that the technical rules are fulfilled.

The dynamic events include the acceleration event, the skid pad event, the autocross event, and the endurance event. During the acceleration event, the car must accelerate from stand over a distance of 75 m. The objective of the skid-pad event is to measure the car's cornering ability by driving through two pairs of concentric circles in a figure of eight pattern. The autocross course consists of different constant and hairpin turns, straights, and slaloms, on which the car must demonstrate maneuverability and handling qualities. During the endurance event over a distance of 22 km, the overall performance of the car, and its durability, reliability and energy efficiency is evaluated.

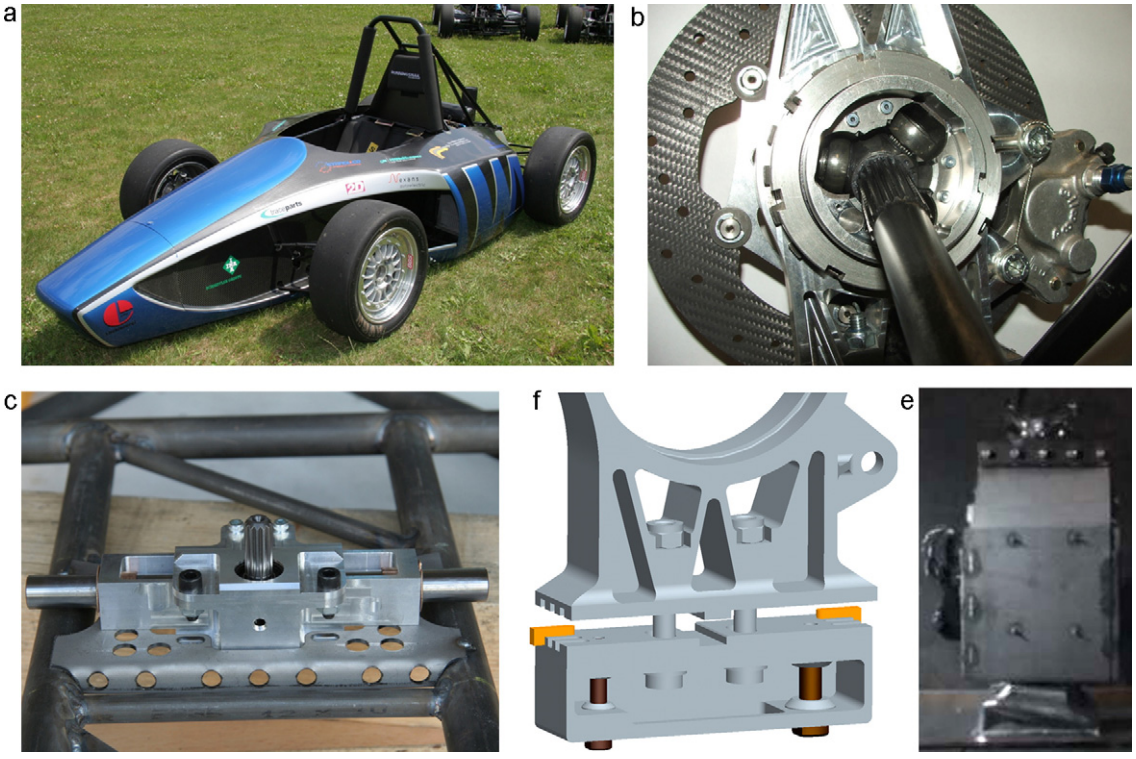

Fig. 12. Mechanical highlights of the racing car: (a) the RS07 model. (b) Aluminum wheel hub on rear suspension with steel inserts. (c) Rack-and-pinion steering gear box. (d) Axle leg with camber adjustment. (e) Crash box test in the drop tower.

Since 2005, the so-called "Running Snail Racing Team" of the UAS in Amberg has participated in competitions in England, Italy, and Germany, and was awarded by the "Best European Newcomer Trophy" in England 2005. At the end of 2009, the UAS team decided to build their first all-electric car based on the RS07 car of 2007, shown in Fig. 12(a). As all formula student cars, it is characterized by open wheels and an open cockpit. At the front and the rear, the car is equipped with a fully operational suspension system including shock absorbers, as well as antiroll bars providing sufficient wheel travel while driving over the race course.

4.1.2. Safety frame, propulsion and braking system

As the most formula student cars, "RS07" is driven at the rear axle. The steering gear is a student-designed rack-and-pinion steering and it is positioned in the lower part of the front suspension; cf. Fig. 12(b).

The three-part aluminum–magnesium rims are mounted on hollow wheel hubs with a large outer diameter to withstand the considerable forces at the wheels; cf. Fig. 12(c). On each wheel hub, a brake disk is floating mounted, activated by a two-piston caliper. The brake calipers are activated via two independent hydraulic circuits, so that, in the case of leak or failure at any point in the system, effective braking power is maintained on at least two wheels.

The wheel hubs are equipped with ceramic hybrid bearings including silicon nitride balls, drastically reducing friction. The wheel hubs run in self-made, very stiff axle legs from aluminum (AW-7075), insuring high mechanical integrity.

In the front and the rear, double wishbone suspensions reside, with unequal length A-arms. Whilst at the front suspension, the spring damper units are actuated by pull rods, at rear, they are activated by push rods. As there are various possibilities to setup the suspensions, special attention has been paid to the camber adjustment that works by means of a predefined "groove-spring-connection" as shown in Fig. 12(d).

The space frame with steel tubes guarantees good maintainability, especially as diverse changes are required by the changeover from the combustion engine to the electrical drive. Two roll hoops are integrated in the frame to prevent the driver from any contact to the pavement during the (unlikely) case of a rollover. The impact attenuator, mounted at the front side, has been proved to withstand when the car crashed against a non-yielding barrier at a speed of $7\,m\,s^{-1}$. In a drop tower, we have demonstrated that the average deceleration does not exceed 20 g, with a peak deceleration less than or equal to 40 g, as shown in Fig. 12(e).

The power from the electric motor is transferred by a two-stage chain gear to the torsion limited-slip differential. The drive shafts connect the differential via constant-velocity joints to the wheel hubs at the rear. The beneficial large-diameter wheel hub, allows to directly integrate the CV-joint into the wheel hub. This measure saves weight, decreases the number of parts, and increases the stiffness of the wheel carrier. In order to insure the aluminum wheel hub to withstand the high Hertzian stress, hardened inserts have been used at the contact points with the CV-joint.

5. Conclusions

We were able to demonstrate the feasibility of a small electric race car based on a hybrid system of lithium-ion batteries and supercapacitors.

(1) None other battery system than lithium-ion is able to meet the demand of low mass and low volume of the vehicle's propulsion system.
(2) In race cars with limited envelope, the recuperation of braking energy is mandatory to limit the weight increase by the batteries.
(3) For this application a battery–supercapacitor hybrid system is superior compared to a stand-alone battery system. The DC-Link currents are smaller (rms and average), and lower effective power losses occur across the resistive elements in wirings, electronics and storage packs.
(4) The battery–supercapacitor hybrid system exhibits lower peak currents and voltage ripple due to low-pass filter behavior, in contrast to the pure battery system. This extends the service life of the electronic inverter components, reduces electromagnetic interference, and avoids the risk of undervoltage dropouts.
(5) With a supercapacitor bank, a complicated battery management system (BMS) is not strictly required. Battery monitoring is recommended, but charging circuits may be omitted during the race.
(6) In the recuperation mode, the supercapacitor module is fast enough to accept short-time high-power pulses without damage.

Acknowledgement

This work is dedicated a team of undergraduate students around Till Ostermann (battery technology).

References

[1] P. Kurzweil, K. Brandt, in: J. Garche, Ch. Dyer, P. Moseley, Z. Ogumi, D. Rand, B. Scrosati (Eds.), Encyclopedia of Electrochemical Power Sources, vol. 5, Elsevier, Amsterdam, 2009, pp. 1–26.
[2] J. Li, E. Murphy, J. Winnick, P.A. Kohl, J. Power Sources 102 (2001) 302–309.
[3] P. Kurzweil, in: J. Garche, C. Dyer, P. Moseley, Z. Ogumi, D. Rand, B. Scrosati (Eds.), Encyclopedia of Electrochemical Power Sources, vol. 1, Elsevier, Amsterdam, 2009, pp. 607–633.
[4] P. Kurzweil, M. Chwistek, J. Power Sources 176 (2008) 555–567.
[5] P.W. Ruch, D. Cericola, A. Foelske, R. Kötz, A. Wokaun, Electrochim. Acta 55 (7) (2010) 2352–2357.
[6] P. Kurzweil, unpublished results.
[7] T.A. Smith, J.P. Mars, G.A. Turner, Proc. IEEE 33rd Annual Power Electronics Specialists Conference 1, 2002, pp. 124–128.
[8] D. Cericola, P.W. Ruch, R. Kötz, P. Novák, A. Wokaun, J. Power Sources 195 (2010) 2731–2736.
[9] Pavithra, Siemens, Sinumerik & Sinamics, Equipment for Machine Tools Catalogue NC 61, Siemens Press, Erlangen, Germany, 2010, pp. 7/122–7/132.
[10] I. Boldea, S.A. Nasar, Electric Drives, CRC Press, Boca Raton, Florida, 2006.
[11] C. Lynch, Electrical Machines, European Patent, EP 0 736 232 B1, 1999.
[12] Bosch-Rexroth, Project Planning Manual, Rexroth Press, Lohr, Germany, 2003, pp. 4.4–4.12.
[13] Tokyo University of Science, World's First HEV Motor Developed without Permanent Magnets, 2009, www.tus.ac.jp/tlo/english/information/pdf/2009/20091216press.pdf.
[14] G. Rolim, Investigation of a drive system. Soft-switching converter and switched reluctance motor, Ph.D. Thesis, Technical University of Berlin, 1997.
[15] PML FlightLink Ltd., EW Series Wheel Motor, Company Brochure, PML FlightLink Ltd., Hampshire, 2010.
[16] Cadence, PSpice User's Guide, Version 10.0, Company Brochure, San Jose, 2003.
[17] A123 Systems, High Power Lithium Ion ANR26650, Company Brochure, Watertown, 2010.